Fuel 400 (2025) 135776

Contents lists available at ScienceDirect

Fuel

journal homepage: www.elsevier.com/locate/fuel

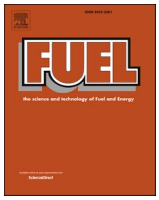

Full Length Article

Chemical recycling of refrigerator plastic waste by pyrolysis: Yields, product composition, and potential applications☆

Jonas Vogt [a], Axel D. Renno [b], Margret Fuchs [b], Tim Kurtz [a], Niklas Netsch [a], Frank Richter [a], Grazyna Straczewski [a], Britta Bergfeldt [a], Yuleika Carolina Madriz-Diaz [b], Andréa de Lima Ribeiro [b], Doreen Ebert [b], Salar Tavakkol [a,*], Simone Raatz [b], Dieter Stapf [a]

[a] Karlsruhe Institute of Technology (KIT), Institute for Technical Chemistry, Hermann-von-Helmholtz-Platz 1, Eggenstein-Leopoldshafen 76344, Germany
[b] Helmholtz Zentrum Dresden-Rossendorf (HZDR), Helmholtz-Institute Freiberg for Resource Technology (HIF), Chemnitzer Str. 40, Freiberg 09599, Germany

ARTICLE INFO

Keywords:
Mixed plastic waste
Chemical recycling
Pyrolysis
Circular economy
WEEE
Refrigerator waste

ABSTRACT

Recycling is crucial for sustainable resource management including heterogeneous and contaminated waste fractions such as those derived from composite materials. This study examines the potential application of pyrolysis of a plastic-rich heterogeneous fraction from an advanced mechanical recycling cascade of refrigerators as a representative example of challenging waste streams from Waste Electrical and Electronic Equipment (WEEE). Advanced spectroscopic and chromatographic techniques are used for feedstock and pyrolysis product characterization. A screw reactor on pilot-scale is used to derive pyrolysis mass balances and to evaluate product yields. The organic condensate with a yield of 64 wt% is rich in styrene and lower aromatics. After further upgrading and separation, aromatic base chemicals and other fractions derived from the organic condensate could substitute fossil feedstocks in the chemical industry. The gas fraction yielding 13 wt% could also be suitable for producing basic chemicals after post-processing. Solid residues enriched with fillers and metals which account for 19 wt% of the pyrolysis products offer recycling opportunities although detailed concepts for pollutant removal and filler reuse remain to be validated. This study highlights the potential of pyrolysis for chemically recycling heterogeneous plastic-rich waste by presenting insights into feedstock and pyrolysis product characterization and by indicating sustainable recycling pathways.

1. Introduction

The widespread use of plastic in various applications has led to a growing problem of plastic waste [1]. The major part of this waste is incinerated, leading to greenhouse gas emissions [2]. Therefore, expanding plastics recycling is essential for a more sustainable future resource management [3]. However, recycling becomes challenging when dealing with heterogeneous waste fractions from a combination of materials, so-called composites. These composites often include different plastic types and contaminants like metals and minerals [4,5].

Mineral contaminants in plastic waste often originate from mineral fillers incorporated into polymers. These fillers are added for several reasons, ranging from the adjustment of mechanical and optical properties of the polymer, improvement of degradation resilience, to cost reduction by decreasing the amount of polymer necessary in the plastic material. Fillers are present as whiskers, particles, or fibers [6]. Most

Abbreviations: ABS, Acrylonitrile butadiene styrene; Br-ABS, Brominated acrylonitrile butadiene styrene copolymer; BTEX, Benzene, toluene, ethylbenzene, xylenes; C-IC, Combustion ion chromatography; DTG, Derivative thermogravimetry; FID, Flame ionization detector; GC, Gas chromatography; HBCD, Hexabromocyclododecane; HSI, Hyperspectral imaging; LCA, Life cycle assessment; LHV, Lower heating value / net calorific value; MMI, Multimode inlet; MS, Mass spectrometer; MWIR, mid-wave infrared; MWL, Minimum wavelength; NCD, Nitrogen chemiluminescence detector; NIST, National Institute of Standards and Technology; NMR, Nuclear magnetic resonance; PC, Polycarbonate; PE, Polyethylene; PET, Polyethylene terephthalate; PMMA, Poly(methyl methacrylate); PP, Polypropylene; PS, Polystyrene; PVC, Polyvinyl chloride; SWIR, Short-wave infrared; TBBPA, Tetrabromobisphenol A diglycidyl ether; TCD, Thermal conductivity detector; TGA, Thermogravimetry analysis; TMS, Tetramethylsilane; VIS, Visible spectrum; WEEE, waste of electrical and electronic equipment; XRD, X-ray diffraction; XRF, X-ray fluorescence.

☆ This article is part of a special issue entitled: 'INFUB14' published in Fuel.

* Corresponding author.
E-mail address: salar.tavakkol@kit.edu (S. Tavakkol).

https://doi.org/10.1016/j.fuel.2025.135776
Received 1 December 2024; Received in revised form 3 May 2025; Accepted 20 May 2025
Available online 12 June 2025

commonly, natural minerals are used as fillers [7,8].

Other common contaminants are halogens like chlorine or bromine stemming from either PVC or brominated flame retardants, especially in engineering plastics [9]. The chemical industry has strict specifications for halogens in their organic feedstocks [10]. In steam cracking for example, the limit falls in the ppm range, while in waste of electrical and electronic equipment (WEEE), bromine can be found at levels in the percentage range [11]. As waste is an inhomogeneous feedstock, the bromine content depends on the specific waste fraction. However, a significant reduction in bromine content compared to the feedstock remains essential [10].

Pure plastic fractions can be recycled mechanically. Plastics that are contaminated, either with other polymers or with other inorganic materials, cannot be recycled mechanically [12]. Metals, minerals, and undesirable elements like chlorine or bromine from, e.g., polyvinyl chloride (PVC) and flame retardants, respectively, represent such contaminations. However, these waste fractions can be recycled chemically, e.g., using pyrolysis or gasification [12]. In chemical recycling processes, the polymers decompose into low molecular weight hydrocarbons. These hydrocarbons may replace fossil feedstocks in the chemical industry, assuming a specified feedstock quality is maintained [10]. This potentially allows the recycling of polymer waste into virgin-quality polymer.

This work is a continuation of the work of Paz et al. (2024) [5] with the goal of the recycling of refrigerators as a representative example of such difficult-to-recycle heterogeneous waste. Mechanical and thermochemical processing includes different steps in recycling. In the work of Paz et al. (2024), firstly, the refrigerators were dismantled by hand to remove harmful substances and recover the valuable electrical components as far as possible. Then, the various metals, including steel and aluminum, glass, and various plastics, were shredded and mechanically separated [5]. The quantitative analysis of this mechanical recycling cascade is shown in Fig. 1. Approx. 23 wt% is obtained as a contaminated heterogeneous plastic-rich waste fraction and used as feedstock in the current study.

Because of the feedstock's inhomogeneity, pyrolysis has been chosen as a chemical recycling path as it is a comparatively robust technology [13]. Using pyrolysis, monomers and a crude oil substitute can potentially be recovered [14,15]. Little recent work has been reported concerning the recyclability potential of mixed plastic waste, especially WEEE, into high-value products by applying pyrolysis as a thermal separation and transformation step in the waste-to-materials value chain [16–19].

This study is taking the plastic-rich fraction from Paz et al. (2024) as its starting point for chemical recycling. It exposes the challenges of recovering possible recyclable materials from a real WEEE fraction. The two main focuses are the comprehensive analysis of the inhomogeneous polymer-rich material fraction of unknown composition and the pyrolysis of the material to produce usable streams. For this purpose, various advanced spectroscopic, chromatographic, and chemical methods are employed for in-depth characterization of the feedstock and the pyrolysis products. Mass balances of the pyrolysis are determined. These mass balances and product characterizations enable application-related process optimization and serve as a basis for process chain evaluation.

2. Materials and methods

2.1. Feedstock preparation

The feedstock pyrolyzed in this study represents the plastic-rich fraction from an advanced mechanical recycling cascade of end-of-life refrigerators collected, which was described in detail by Paz et al. (2024) [5]. This plastic-rich fraction accounted for 23.4 wt% of the input introduced to the mechanical recycling and was obtained after dismantling, shredding, and sorting, as shown in Fig. 1. The polyurethane-rich insulation fraction of the refrigerators, which is easier to dismantle, was excluded.

The plastic-rich fraction was shredded to a target particle size of approximately 5 to 30 mm using a 4-shaft shredder RS 30 from Untha before pyrolysis. This preliminary step reduces the particle size, ensuring optimum continuous dosing into the pyrolysis reactor and improved heat and mass transfer during the thermochemical conversion.

2.2. Pyrolysis reactor setup

In this study, a screw reactor is used to pyrolyze the plastic-rich waste, as depicted in Fig. 2. The suitability of the reactor for remarkably heterogeneous plastic waste has already been reported by Netsch et al. (2024) [20]. Its high feedstock flexibility enables the direct generation of pyrolysis products in gaseous and liquid forms. The comprehensive instrumentation and the pilot scale allow a precise mass and energy balance of the system and the generation of representative pyrolysis products. The results provide the basis for calculating downstream techno-economic and ecological evaluations. The reactor incorporates quartz sand as a carrier medium for thermal pyrolysis with a ratio of approximately 4:1 of sand to plastic waste to ensure flowability and reduce the risk of plastic melt blockage and as a moderator medium for uniform heating of the plastic waste making the pyrolysis more

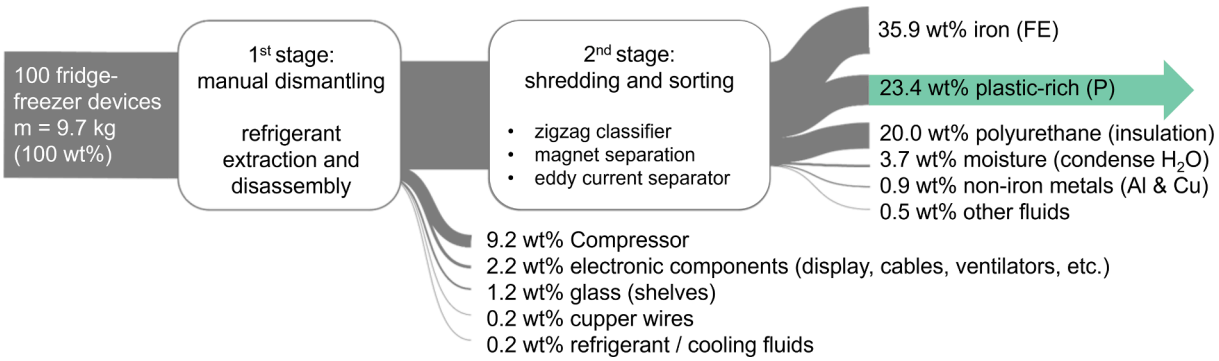

Fig. 1. Mass balance of the dismantling and mechanical processing of cooling appliances by Paz et al. (2024) [5] indicating the processed sub-stream used in the study by a green arrow. (For interpretation of the references to color in this figure legend, the reader is referred to the web version of this article.)

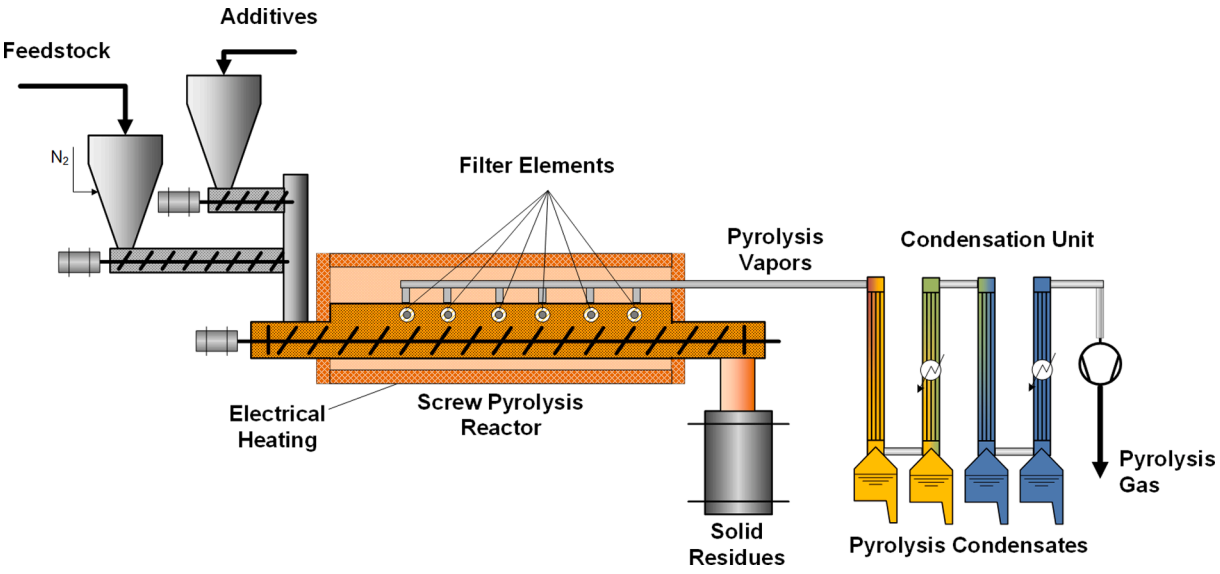

Fig. 2. Scheme of the pyrolysis reactor setup.

controllable. Operating under constant conditions, the reactor maintains a temperature of 450 °C, a solids residence time of 30 min, and a feedstock mass flow rate of approximately 1 kg/h. The experimental duration of 5 h ensures steady-state operation of over 4 h.

The reactor geometry is trough-shaped, with electrically heated walls spanning 2 m. The reactor's temperature is monitored using numerous thermocouples, leading to precise temperature control with a maximum deviation of less than 10 K from the setpoint temperature at all measuring points. Solid residues are efficiently discharged from the reactor into a vessel at the end of the screw reactor via a 150 mm-diameter screw. Evolving pyrolysis vapors pass through ceramic hot-gas filter elements into a two-stage condensation unit. This unit operates at 60 and 5 °C, with each stage consisting of two double-tube heat exchangers followed by electrostatic precipitators. The reactor is continuously flushed with nitrogen to prevent an oxidizing atmosphere and to ensure the rapid discharge of pyrolysis gases and vapors from the hot section. Precise control of the supplied nitrogen is achieved through mass flow controllers (Bronkhorst EL-FLOW Select). The pyrolysis gases leaving the condensation unit are directed through an online gas analysis system and subsequently to a flare for further handling.

The density and calorific value are continuously measured using CWD2000 from UNION Instruments, and the volume flow of permanent gases is continuously measured by the drum-type gas meter TG 20 from Ritter Apparatebau to provide reliable data for mass balancing.

To close the mass balance, the condensate and the solid products were weighed. The accumulated mass of pyrolysis gas was calculated by subtracting the nitrogen mass from the total gas mass which was determined from the measured volume flow (V_{gas}) and the gas density (ρ_{gas}). The nitrogen mass was determined by multiplying the density of nitrogen with the measured nitrogen gas flow ($V_{gas,0}$) before the start of the experiment. The masses of condensate, solid products, and pyrolysis gas were subtracted from the feedstock mass to obtain the loss of mass balance.

$$m_{feedstock} + m_{sand} - \left(m_{pyrolysisgas} + m_{condensate} + m_{solids}\right) = m_{losses} \quad (1)$$

$$m_{pyrolysisgas} = \rho_{gas} \cdot V_{gas} - m_{N2} \quad (2)$$

$$m_{N2} = \rho_{N2} \cdot V_{gas,0} \quad (3)$$

After pyrolysis, the solid products were separated into a fine fraction with a particle size smaller than 0.5 mm, a mid-fraction with a particle size between 0.5 and 2.0 mm, and a coarse fraction with a particle size bigger than 2 mm. From those solid fractions, a sample was taken for further analysis. All gas and condensate samples from three experiments were measured, and the results were used to determine the mean value and the sample standard deviation. For qualitative 2D-GC analysis, the condensate from the second experiment was chosen. The solid product samples from two experiments were analyzed, and the results were averaged. In the latter case, no standard deviation was calculated. The two measurement results were appended to the Supplementary Data.

3. Feedstock and product analysis

Table 1 presents all analyses conducted in this work.

Table 1
Overview of all analyses conducted in this work.

Parameter of interest	Sample type	Analytical method
Polymer type identification	Feedstock	Hyperspectral imaging (HSI)
Elemental composition of C, H, N	Feedstock, organic condensate, solid products	Elemental analysis
Elemental composition of Cl, Br	Feedstock, organic condensate, solid products	Combustion ion chromatography (C-IC)
Decomposition behavior	Feedstock	Thermogravimetric analysis (TGA)
Ash content	Feedstock	Incineration in an oven
Phase composition	Quartz sand, solid products	X-ray diffraction analysis (XRD)
Chemical composition of inorganics	Quartz sand, solid products	Wavelength dispersive X-ray fluorescence analysis (XRF)
Chemical composition of coarse inorganics	Coarse fraction of the solid products	Micro X-ray fluorescence analysis (μ-XRF)
Quantification of selected gaseous compounds	Gaseous products	Micro gas chromatography (μ-GC)
Quantification of selected liquid organic compounds	Organic condensate	GC with a flame ionization detector (GC-FID)
Estimation of bulk chemical composition	Organic condensate	Proton nuclear magnetic resonance analysis (^{1}H NMR)
Identification of liquid organic compounds	Organic condensate	Two-dimensional GC-FID coupled with a mass spectrometer (2D-GC)

3.1. Feedstock analysis

Polymer types in the feedstock were identified using reflectance based hyperspectral imaging (HSI), which combines spectral and spatial information. The analysis utilized a SPECIM SisuROCK drill core scanner with push broom hyperspectral sensors for the shortwave infrared (SWIR) and midwave infrared (MWIR) ranges. A decision tree model was used to classify polymers based on spectral fingerprints. Unique absorption features were linked to molecular modes specific to each polymer type, leading to a SWIR of interest from 1650 to 1750 nm and to a MWIR from 4400 to 4600 nm. Key polymer types (e.g., PE, PET, PC, PVC, PP, and ABS/PS/PMMA) were identified through their diagnostic bands in the SWIR and MWIR ranges.

Pre-processing of hyperspectral data included radiometric/geometric corrections, co-registration, orthorectification, and background masking. Notably, dark background removal also excluded black plastics like PVC wire coverings. To differentiate overlapping fingerprints (e.g., ABS/PS/PMMA), a specific MWIR absorption at 4474 nm was used to identify ABS.

A minimum wavelength mapping (MWL) approach detected the strongest absorption per pixel, feeding into the decision tree to generate polymer classification maps. Polymer surface area was then estimated by pixel counts, acknowledging that occluded particles below the surface could not be detected.

The elemental composition regarding carbon, hydrogen, and nitrogen content was determined using LECO Truspec CHN Micro. The analysis was performed with homogenized feedstock powder, ground solid residues, and organic condensate. The sample mass accounted for 1 to 2 mg. Combustion ion chromatography (C-IC) was carried out with a sample size of 15 to 30 mg to determine the chlorine and bromine content using the AQF-2100 device from a1 environscience GmbH and Thermo Fisher Scientific GmbH. Furthermore, another analysis of carbon, hydrogen, and nitrogen, as well as the halogens chlorine and bromine, was carried out for fine solids following DIN 51732:2014–07 [21], in each case using double analysis and averaging.

Thermogravimetric analysis (TGA) was conducted for laboratory-scale experiments using a NETZSCH TG 209 F1 Libra. A 10.0 ± 0.1 mg sample of the homogenized feedstock powder was introduced in Al_2O_3 crucibles. The pyrolysis was performed with a program ranging from 30 to 600 °C at a constant heating rate of 10 K/min in a nitrogen atmosphere. A combustion step ranging from 600 to 900 °C was conducted by inserting air into the oven. The thermogravimetric analysis was conducted six times and results were averaged to validate reproducibility.

The ash content of the feedstock was determined by burning three batches of 30 g feedstock, each. To achieve controlled incineration, the oven temperature was stepwise increased from 250 °C with a heat rate of 100 K/h and then held at 550 °C for 3 h.

To characterize the chemical composition of inorganic samples, wavelength dispersive X-ray fluorescence (XRF) analyses were conducted using a PANalytical Axios max device equipped with a Rh-tube from Malvern-Panalytical. To prepare glass beads, 1 g of the pre-calcined material was thoroughly mixed with 8 g of LiB_4O_7 as fusing flux and melted in an automatic CLAISSE TheOx oven in platinum crucibles. The data were obtained from the manufacturer's fully calibrated WROXI program. Additionally, 10 g of sample material was thoroughly mixed with 2 g wax (Cereox©) and transformed into a 40 mm pressed pellet. Data was evaluated using the fundamental parameter-based OMNIAN program and for additional elements with the ProTrace program, both provided by Malvern-PANalytical.

The phase composition of the inorganic samples was determined using X-ray diffraction (XRD). Aliquots of around 3 g of the material were used for XRD analysis. XRD measurements were done using a PANalytical Empyrean diffractometer equipped with a Co-tube and a PIXcel 3D medipix 1x1 area detector from Malvern-PANalytical. The tube was operated at 35 kV and 35 mA. The measured 2-theta range was set 5 to 80° at a step size of 0.0131° 2theta. Phase identification was done using the ICDD PDF-4 + database, while quantification was performed via the Rietveld method using the Profex/BGMN v.4.1 software bundle.

Chemical analyses of particles in the solid samples were performed using the M4 TORNADOPLUS Micro X-Ray Fluorescence Spectrometer. For this purpose, a Rh microfocus X-ray tube with an approx. 20 µm spot size diameter was used. Element distribution maps were carried out with individually customized variable time and pixel spacing conditions.

3.2. Gas analysis

Throughout the pyrolysis, quantitative online gas measurements were carried out in a 5 min interval using a gas chromatograph (GC). The Micro GC Fusion by INFICON is equipped with three columns and three micro thermal conductivity detectors (µTCD), enabling the determination of the gas composition. In an Rt-Molesieve with a pore size of 5 Å, the inorganic gases N_2, O_2, H_2, CO, CO_2, and CH_4 are separated from saturated and unsaturated hydrocarbons. The different C_2 and C_3 gases are quantified on the second channel equipped with an Rt-Q-Bond column. Higher boiling C_4 hydrocarbons are separated from unidentified compounds via the Rxi-1 ms on the third µGC channel.

The mass fraction of each gas species x_i was calculated using Eq. 4, considering the volumetric fraction υ_i and the gas density ρ_i at 273.15 K and 101.325 kPa while excluding nitrogen as the flush gas. Gas species that could not be quantified, such as C_{5+} alkanes and alkenes, aromatics, as well as heteroatom-containing hydrocarbons, HCl, HBr, NH_3, or remaining moisture, were not included in the calculation.

$$x_i = \frac{\upsilon_i \cdot \rho_i}{\sum_j \upsilon_j \cdot \rho_j} \quad (4)$$

$$with\ i = H_2, CO, CO_2, CH_4, C_2H_6, C_2H_4, C_3H_8, C_3H_6, C_4H_{10}, C_4H_8$$

3.3. Condensate analysis

The analysis of organic condensates was performed with a flame ionization detector (FID) incorporated in the 7890B GC system from Agilent Technologies. The sample was prepared by diluting the organic condensate with chloroform in a volumetric ratio of 1:9. A Rtx®-DHA-150 column from Restek GmbH with a length of 150 m, an inner diameter of 250 µm, and a film thickness of 1 µm was used. With this exceptionally long column, a good peak separation could be achieved in a runtime of 480 min. Before the analyses, the GC system was calibrated with standards to enable quantification. The amount of n-alkanes and 1-alkenes within the chain length range from C_5 to C_{21} as well as benzene, toluene, ethylbenzene, p-xylene, o-xylene, styrene, α-methylstyrene, cumene, phenol, indene, naphthalene, bibenzyl and stilbene were determined.

A Spinsolve 'MultiX' benchtop nuclear magnetic resonance (NMR) system from Magritek was used to quantitatively differentiate between saturated and unsaturated aliphatic protons, aromatic protons, and protons bound to functional organic groups in the pyrolysis condensate. The NMR system operates with a permanent magnet of 80 MHz. With the ^{1}H NMR method, 480 µL of the sample was mixed with 20 µL of tetramethylsilane (TMS) as a spectral reference substance and measured three times with 16 scans, a repetition time of 15 s, and a pulse angle of 90° with activated ^{13}C decoupling. Data processing includes referencing TMS to a chemical shift of 0 ppm and a polynomial baseline correction.

Two-dimensional gas chromatography (2D-GC) was performed to characterize the main organic compounds in the pyrolysis condensate. The 2D-GC system from Agilent Technologies consists of an 8890 GC system, a 5977B mass spectrometer (MS). For the analysis, 1 µL of analyte is injected into the multimode inlet (MMI) via an automatic autosampler. The sample preparation included diluting homogenized pyrolysis oil in chloroform in a volumetric ratio of 1:9. The first separation column, an Agilent DB-5 ms (20 m in length, 0.18 µm film thickness, diameter of 180 µm), is connected to the MMI via a 50 cm

long deactivated pre-column. A reversed flow modulator with a modulation time of 10 s and an injection time of 0.36 s was used. The modulator transfers the analyte into a second separation column. The second column is a Trajan BPX50 with a length of 5 m, a film thickness of 0.25 μm and a diameter of 250 μm. After leaving the GC separation unit, the sample stream is divided with a splitter (ratio of 1:10) into a stream for the quadrupole MS for the identification of unknown components and into a stream for the FID for the detection of hydrocarbons in a wide concentration range. Data evaluation was carried out using the GC Image software. A two-dimensional plot was created, where the measured mass spectrum of every peak was then compared with the NIST database.

4. Results

4.1. Feedstock analysis

A detailed assessment of the feedstock composition was performed on a representative material sample of 5 kg. A manual picking inspection was conducted to identify the suitability of the feedstock for pyrolysis in a screw reactor. As plastic particles represent the highest mass content among classes with 86.1 wt%, a sufficiently high organic content can be assumed. Despite prior mechanical sorting, metals, and wire pieces, consisting of a metallic core and a plastic wire jacket, were still identified in the plastic-rich fraction with a share of 13.7 wt%. A breakdown of the various visually different components can be found in the Supplementary Data Apart from the metal fraction, a more detailed analysis was required to determine the relative contributions of different polymer types in the plastic-enriched fraction.

SWIR HSI analysis confirms the successful spectral-based polymer classification of 87 % of the analyzed surface area, allowing for the identification of PC, PE, PET, PP, ABS/PS/PMMA, and PVC. The unknown fraction with a surface area of 14 % remained unclassified due to either the absence of diagnostic features matching the abovementioned polymer classes or low reflectance signals within the selected spectral regions. The spectral-based classification map, which is shown in Fig. 3, displays the recorded distribution of polymer classes in the plastic-rich feedstock fraction. A general overview indicates that the polymer types are distributed independently of particle size. The relative surface areas associated with the main polymer classes in the feedstock were PC (35 %), ABS/PS/PMMA (26 %), and PP (21 %). Only small fractions of particles belong to the classes of PVC (2 %), PE (2 %), and PET (0.2 %).

The composite class of ABS/PS/PMMA is further resolved using MWIR, differentiating between ABS in pure form or as a copolymer. The fraction of pixels, containing either ABS, ABS/PS, or ABS/PMMA account for 17 % of the total surface area, while the remaining 9 % can be allocated to PS or PMMA in pure form or as copolymers. The combined SWIR-MWIR analysis additionally revealed the coexistence of PC and ABS in particles, with 34 % of the surface area being further characterized as ABS/PC composites and only 1 % representing pure PC.

The feedstock was tested for its elemental composition. The results are listed in Table 2. Elevated heteroatom contents for nitrogen, chlorine, and bromine are determined.

The feedstock-specific degradation behavior is characterized using thermogravimetric analyses. Fig. 4 depicts the temperature-dependent average volatile formation as a bold black line with the standard deviation represented by the grey area. The volatile formation rate in wt %/min is displayed as a dashed line. The feedstock decomposes in several reaction steps at different temperatures. The volatile formation rate results from the derivative thermogravimetry (DTG) represents the mass change derivative as a temperature function. The volatile formation rate emphasizes the distinct reaction steps. The first decomposition step takes place at temperatures between 250 to 300 °C. Only a minor amount of about 5 wt% volatiles are formed.

Between 350 and 480 °C a second decomposition step could be identified accounting for approximately 75 wt% of the volatiles.

After adding oxygen at 600 °C, the ash content of 10.1 ± 6.4 wt% could be determined. The standard deviation reflects the sample's heterogeneity. The incineration of 90 g feedstock in the muffle furnace compensates for this effect. The incineration resulted in 10.5 ± 1.0 wt% for the ash content, confirming the average value obtained by TGA.

Table 2
Measured elemental composition of the plastic-rich waste fraction.

Element	C	H	N	S	Cl	Br
Units	wt%	wt%	wt%	wt%	mg/kg	mg/kg
Composition	79.1	9.2	1.21	< 0.1	26300	2160
Standard deviation	4.9	1.3	0.34	–	6700	300

4.2. Mass balance

Three identical experiments with plastic-rich waste were performed. The mass balance differentiating between the solid, condensable, and gaseous products is shown in Fig. 5. The organic condensate phase accounts for 64.2 wt% representing the major product fraction, followed by 18.6 wt% of solid products and 12.9 wt% of gaseous products. The condensates were separated into an organic and aqueous phase using a decanter. However, the proportion of the aqueous phase is almost negligible. The solid products can be further identified as 8.1 wt% carbonaceous solid, also referred to as char, and 10.5 wt% of ash, assuming that the ash-forming components are also present as ash after pyrolysis in a nitrogen atmosphere. Despite working with an inhomogeneous feedstock, high reproducibility of the mass balance is verified by a low standard deviation of a maximum of approx. 3 wt% for pyrolysis gas.

4.3. Solid products

Fig. 6 shows the different solid streams entering and exiting the pyrolysis reactor as well as the post-treatment of those streams. The solid products were separated into three fractions by sieving. Apart from their different particle sizes, the three fractions are also distinguished by their respective compositions and properties. The mid fraction, ranging from 0.5 to 2 mm in particle diameter, mainly consists of the sand introduced into the pyrolysis process. It is therefore referred to as sand fraction in the following. The fine fraction with a particle diameter smaller than 0.5 mm primarily comprises fine char particles, abraded sand, and

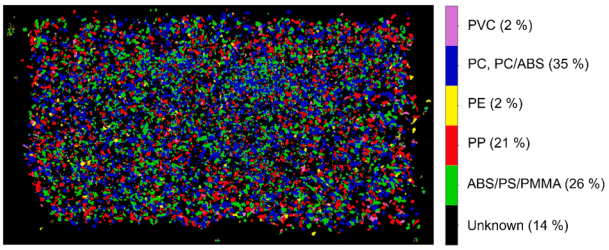

Fig. 3. Plastic type classification based on SWIR HSI data of the plastic-rich waste fraction.

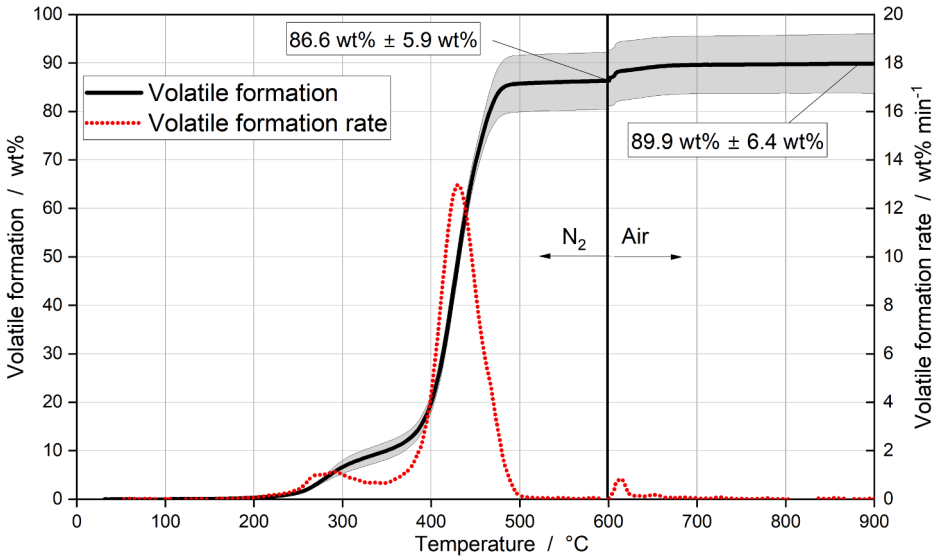

Fig. 4. Volatile formation (compact line) and volatile formation rate (dashed line) determined for the plastic-rich waste fraction using TGA at a constant heating rate of 10 K/min.

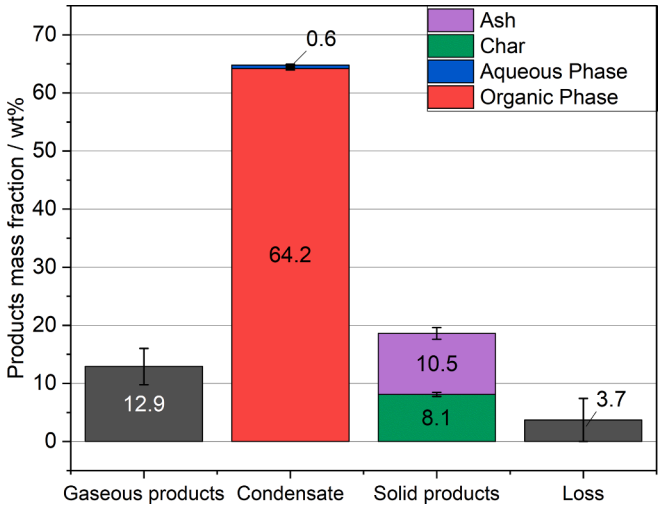

Fig. 5. Mass balance of the pyrolysis experiments.

mineral plastics additives. The coarse fraction differs significantly in composition with its pieces of metal and glass featuring a particle diameter higher than 2 mm, such as copper wires, sheet metal, and glass.

After pyrolysis, the solid residue comprised 95.9 wt% quartz sand and 4.1 wt% of other products. Considering the 8.1 wt% of char produced during pyrolysis, a char content of 1.8 wt% of all solids including the quartz sand, leaving the pyrolysis reactor including the quartz sand was calculated.

As the sand fraction mainly consists of quartz sand used as a carrier medium, the focus of this work was on analyzing the fine and coarse fractions, as these fractions mainly consist of solid products from pyrolysis of the feedstock used. A detailed analysis of the sand fraction is provided in the Supplementary Data.

4.4. *Fine fraction*

An XRD analysis was carried out to determine the composition of the fine fraction. The results are shown in Fig. 7 (a). Calcite, rutile, and talc represent the main components, accounting for 82.6 wt%. Due to the selected XRD method, it is impossible to differentiate between copper, iron, and zinc. Therefore, the value for copper of 1.8 wt% may also contain other metals. Minor amounts of halite are identified. Apart from the calcite and rutile components, the standard deviation of the XRD

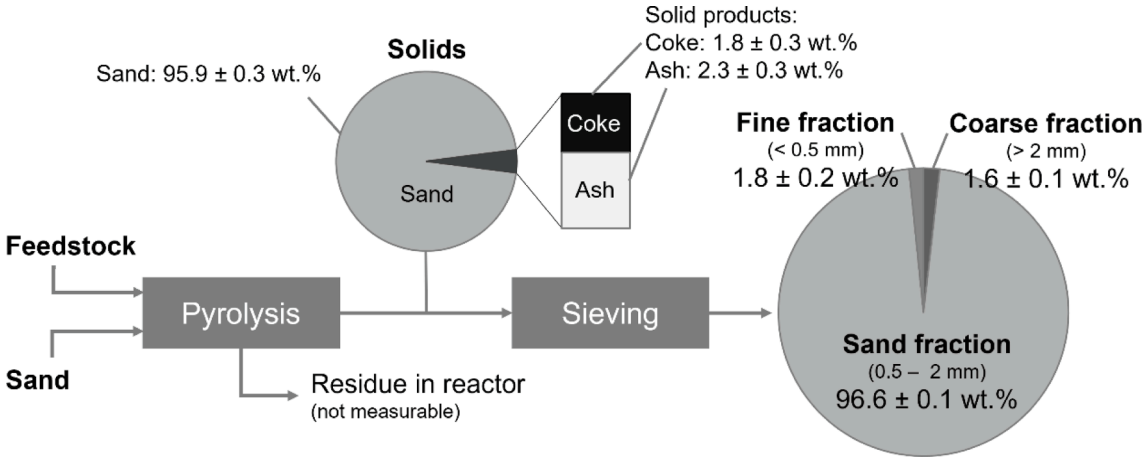

Fig. 6. Solid streams in the pyrolysis process including the composition of the solid residue after pyrolysis and after sieving specified by particle diameter fractions.

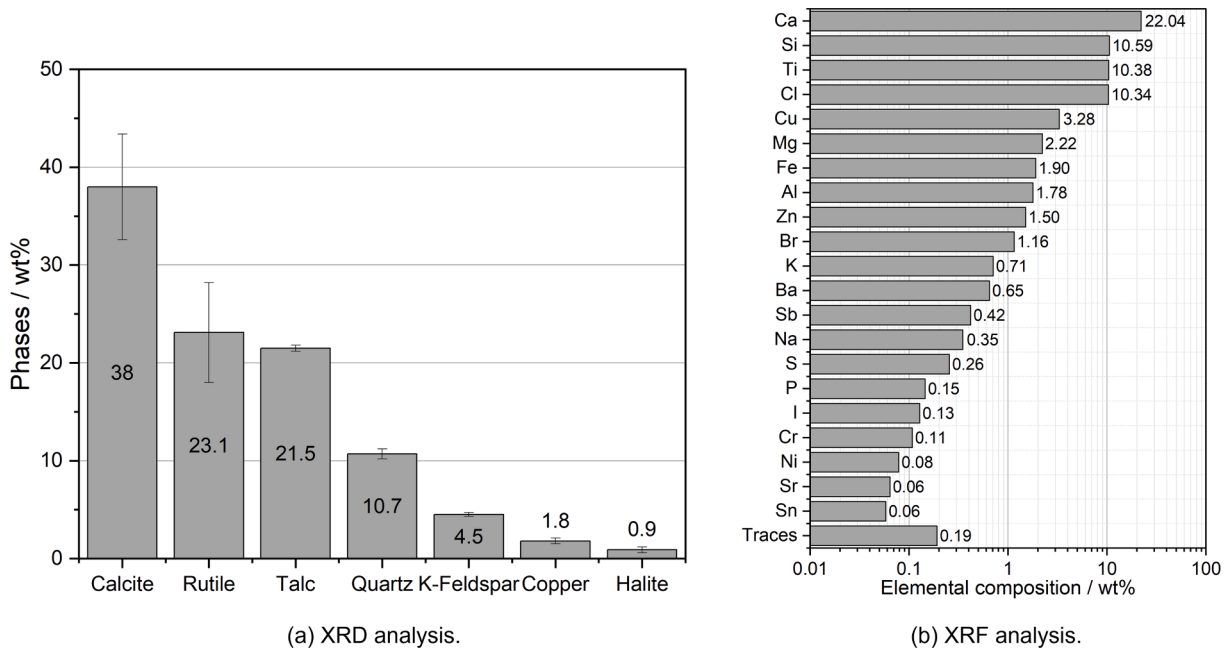

Fig. 7. XRD and XRF analysis of the fine fraction for phase and elemental composition. Trace elements (< 0.05 wt%) by XRF analysis include W, Nd, Mn, Pb, Zr, Co, Nb, As, Mo.

measurement is exceptionally low. However, only the crystalline phases can be detected with XRD, meaning that char and other amorphous materials are not considered. Elemental analysis of the fine fraction was conducted to determine char and other compounds. The fine fraction consists of 20.6 ± 1.1 wt% carbon, 1.0 ± 0.1 wt% hydrogen, 0.6 ± 0.0 wt% nitrogen, 39200 ± 640 mg/kg chlorine, and 3900 ± 80 mg/kg bromine. Using XRF analysis of pressed pellets, 68.5 wt% of the elements present in the fine fraction could be determined, as shown in Fig. 7 (b). Calcium with 22 wt%, silicon, titanium, and chlorine, each with approx. 10 wt% are the main elements in the fine fraction. Other elements, such as copper, magnesium, aluminum, iron, zinc, and bromine, together make up approx. 12 wt% of the fine fraction. The remaining 21 detected elements, such as potassium, barium, and sodium, are all detected in a share of less than 1 wt% each and comprise 3 wt% of the fine fraction.

4.5. Coarse fraction

Before the coarse fraction was examined in detail, it was separated into a first coarse fraction with a particle diameter between 2.0 and 3.5 mm, which accounted for 62 wt% of the total coarse fraction, and a second coarse fraction featuring a particle diameter higher than 3.5 mm with a share of 37.6 wt% and a loss of 0.4 wt% due to the separation process. The second coarse fraction was then sorted into magnetic metals, non-magnetic metals, wires, glass, pyrolysis residues, and others (see Fig. 8) using the criteria from Paz et al. 2024 [5]. Using μ-XRF analysis, it was shown that a large proportion of the particles defined as wire consist of copper alloys and that small amounts of a Ni-Cu alloy are also present. The main components of the magnetic metals showed variations in steel composition, with iron as the main element and chromium and nickel as alloy additives. Noteworthy in this regard is the detection of contaminants such as chlorine and bromine. The non-magnetic metals predominantly consisted of aluminum, with residues of brass alloy.

4.6. Gas composition

The permanent gas contains hydrocarbons of short chain length and inorganic gases, including N_2, CO_2, CO, and H_2. The hydrocarbons feature a boiling point below or in the range of the second condensation

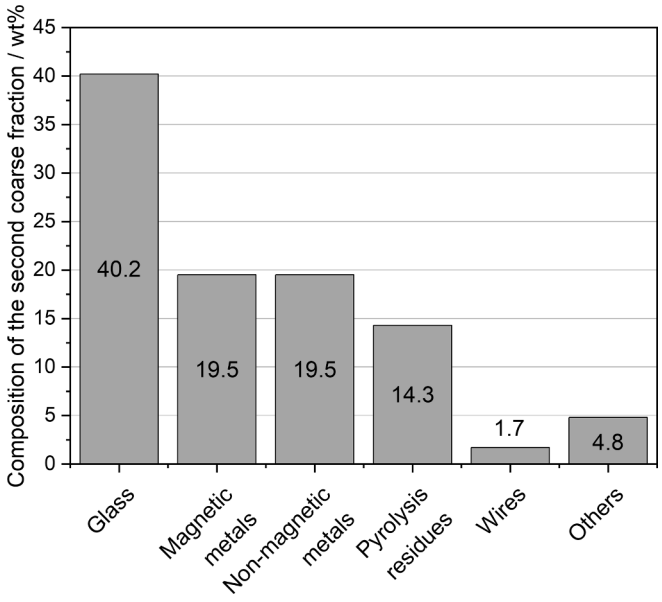

Fig. 8. Breakdown of the second coarse fraction (> 3.5 mm) into six material groups.

stage temperature of around 5 °C. For their quantification, ten compounds were calibrated, which make up 1.6 vol% of the permanent gas stream. A major part of the gas accounts for N_2 as the flush gas with 95.8 vol%. Thus, 2.5 vol% of the gaseous species were not quantified and are attributed to the balance loss when closing the gas balance. About 42 wt % of the identified gases comprise CO_2 (see Fig. 9). Moreover, 43.5 wt% of the compounds identified in the gas are alkenes, and 13.2 wt% are alkanes in the carbon chain length of C_1 to C_4. Only minor proportions of CO and H_2 are quantified.

4.7. Organic condensate composition

Following the operation mentioned above, the pyrolysis of the

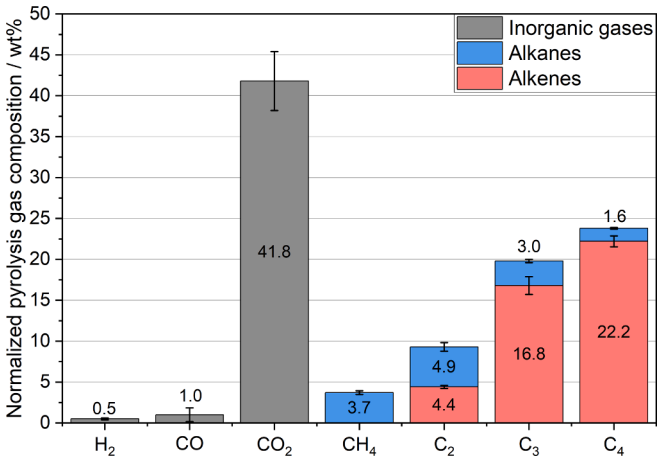

Fig. 9. Normalized pyrolysis gas composition with subdivision of $C_2 - C_4$ hydrocarbons into alkanes and alkenes. Values are normalized to 100 wt%.

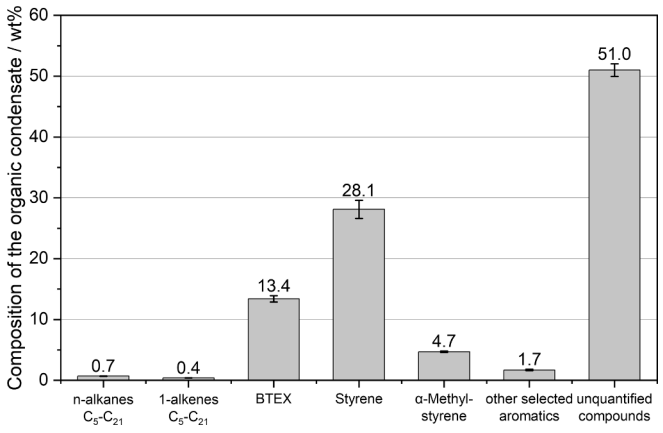

Fig. 10. Composition of the organic condensate analysis using GC-FID.

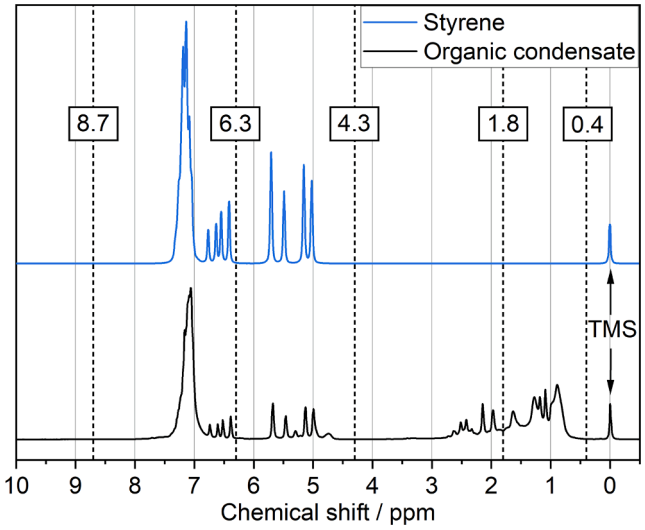

Fig. 11. ^{1}H NMR spectrum of pure styrene and of the organic condensate generated in the pyrolysis experiments.

plastic-rich fraction yielded 64.2 wt% of organic condensate. The elemental analysis of this primary product is listed in Table 3. The organic condensate consists of 86.3 wt% carbon and 9.0 wt% hydrogen. Considering the molar ratio of hydrogen to carbon of 1.25 mol H / mol C, there is a trend towards a highly aromatic character of the condensate. Nitrogen (0.83 wt%), chlorine (515 mg/kg), and bromine (188 mg/kg) are present.

Using GC-FID analysis of the organic condensate, 49 wt% of the condensate could be assigned to quantified compounds. The analysis revealed the dominant presence of aromatic molecules, as shown in Fig. 10. Especially styrene, which represents the monomer of PS and ABS plastics, accounts for 28.1 wt%. With an amount of 4.7 wt%, α-methylstyrene represents another characteristic product of polystyrene pyrolysis. Furthermore, BTEX, with a total amount of 13.4 wt%, comprises 9.3 wt% ethylbenzene, 4.0 wt% toluene, and 0.1 wt% benzene and xylenes. However, a considerable proportion of paraffinic compounds are detected, indicating the diverse polymer composition of the feedstock. Other selected aromatics make up 1.7 wt% of the organic condensate with 0.9 wt% cumene, 0.3 wt% phenol, 0.2 wt% bibenzyl, 0.1 wt% stilbene, 0.1 wt% indene, and 0.1 wt% naphthalene.

More information on the composition of the organic condensate is provided by ^{1}H NMR spectroscopy. In contrast to GC-FID, the analysis offers the advantage of independence from calibrated compounds, resulting in the entire condensate being included in the quantitative determination. Fig. 11 shows the ^{1}H-spectrum of pure styrene and the organic condensate. The similarity of the peaks of both samples at the chemical shift of 4.9 to 7.5 ppm is noticeable, which can be explained by the high styrene concentration in the organic condensate. However, other peaks at the chemical shift of 0.5 to 2.7 ppm can be observed in the ^{1}H-spectrum of the organic condensate. These peaks indicate aliphatic protons. The allocation of the peaks to areas of defined functional groups was carried out using the chemical shift assignments reported by Skoog et al. (2013) and Hesse et al. (2012) [22,23]. A detailed categorization of the functional group sections can be found in Fig. 12.

The result shows that in addition to 42.2 mol% of the protons that can be allocated to an aromatic group, 34.2 mol% of the protons can be allocated to an aliphatic group (0.4 to 1.8 ppm). This group comprises CH, CH_2, and CH_3 fragments surrounded by other aliphatic groups, such as paraffins. The protons within the chemical shift range of 1.8 to 4.3 ppm can be allocated to an aliphatic group close to a functional group. This can be, for instance, a methyl or ethyl group attached to an aromatic ring.

Another 10.4 mol% of the protons within the organic condensate can be allocated to the olefinic range from 4.3 to 8.7 ppm chemical shift. Functional groups in the range of the chemical shift of 8.7 to 13.0 ppm featuring oxygen content, such as an aldehyde or carboxyl group, cannot be detected.

Elemental and ^{1}H NMR analyses indicate various aliphatic compounds present in the condensable product but not detected by GC-FID. 2D-GC enables the precise identification of these and more compounds, using MS data processing. Fig. 13 displays the two-dimensional projection of the three-dimensional chromatogram. The x-axis represents the retention time on the first non-polar column, while the y-axis shows the retention time on the second polar column. The polarity of the analytes increases in the vertical direction, while the molecular weight of the substance or boiling point increases with the horizontal position of higher retention times. The peak intensity and, thus, the concentration of a component in the sample is highlighted by color to simplify the diagram to a two-dimensional plot.

For the identification of the unknown organic compounds the 2D-GC analysis enables a distinction between paraffins, monoaromatics,

Table 3
Measured elemental composition of the organic condensate.

	C	H	N	Cl	Br
Units	wt%	wt%	wt%	mg/kg	mg/kg
Composition	86.3	9.0	0.83	515	188
Standard deviation	1.9	0.4	0.04	8	4

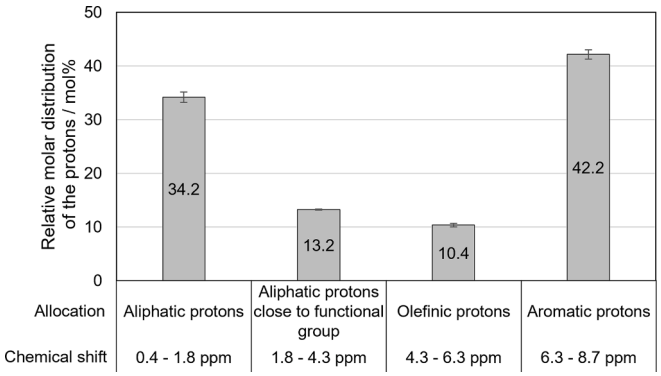

Fig. 12. Allocation of measured protons in the organic condensate to functional groups.

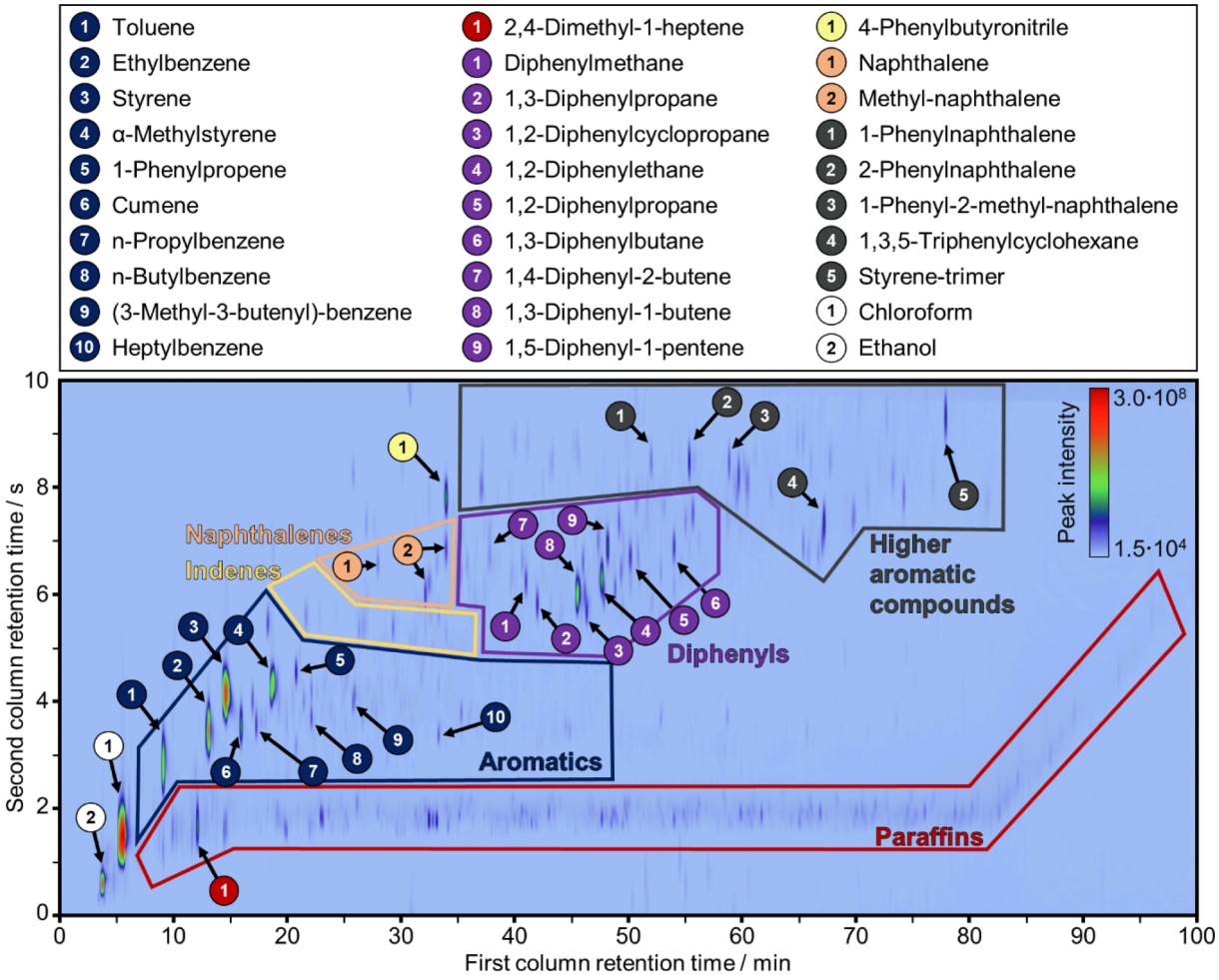

Fig. 13. Chromatogram showing the 2D-GC analysis of the organic condensate produced in the second pyrolysis experiment.

indenes, naphthalenes, diphenyls, and organic molecules with three or more conjugated or non-conjugated aromatic rings. In addition, the peaks with the highest peak intensities are shown in the diagram using the substance groups listed above. They represent the main components of the pyrolysis condensate.

5. Discussion

5.1. Feedstock characterization and pyrolysis

The manual picking inspection of the feedstock displays its heterogeneity. The separation of material types during shredding and sorting fails to achieve sufficient enrichment of plastics. A considerable share of 13.7 wt% of metal products demonstrates this.

The elemental analysis of the feedstock helps estimate the expected organic products and solid residue yields. The low ash content of 10.5 wt % demonstrates the potential for material recovery in chemical recycling. Combined with the determination of the ash content, a high carbonaceous content of pyrolysis condensate and pyrolysis gas can be expected. The amount of nitrogen, chlorine, and bromine indicates that extensive post-treatment of the pyrolysis products will be necessary to remove the heteroatoms before their utilization because of contamination limits.

A detailed breakdown of the plastic types is obtained by performing

reflectance spectroscopy-based classification using a combined SWIR-MWIR analysis of the feedstock. Since the pyrolysis mechanism and the product yields and compositions are highly polymer-dependent, this analysis helps to preliminary estimate the feedstock applicability to pyrolytic processes [20]. As the data only allows the surface areas and not the mass share of polymers to be measured, and the fact that black plastics were excluded from the HSI analysis, slight deviations from other quantification methods are to be expected. For example, in the case of PVC, deviations between the value determined by the HSI analysis (2 %) and the theoretical PVC content from the elemental analysis differ. With a chlorine content of approx. 2.6 wt%, a PVC content of about 5.8 wt% is expected. The theoretical PVC content was calculated assuming the theoretical chlorine content in PVC of 56.8 wt% [24]. In addition, the potential use of plasticizer (40 wt% of PVC), which occurs in flexible or elastomeric applications such as PVC wire jackets, was considered [25].

The TGA provided data on the feedstock's thermal decomposition, enabling estimations of the required pyrolysis temperature concerning adequately rapid degradation kinetics. The first decomposition step can be allocated to the dehydrochlorination of PVC forming HCl, polyene structures, and, to a smaller extent, benzene, naphthalene, and phenanthrene molecules through Diels-Alder reactions and successive dealkylation of polyene molecules [26,27]. The decomposition of brominated flame retardants, such as the most commonly used tetrabromobisphenol A diglycidyl ether (TBBPA) and hexabromocyclododecane (HBCD), can also be assigned to this temperature range. TBBPA decomposes at about 185 °C, and decomposition intensifies at about 250 °C [28]. HBCD is used in PS and forms HBr at temperatures between 180 to 240 °C [29]. The decomposition of brominated acrylonitrile butadiene styrene copolymer (Br-ABS) cannot be assigned to this temperature range, as it decomposes between 350 to 470 °C [30]. Brominated flame retardants are often used in housings of electrical and electronic parts [31]. The second and major decomposition step between 350 and 480 °C can be attributed to the decomposition of the PS, ABS, and PP, as they show similar decomposition behavior in this temperature range [20].

5.2. Solids

Solid products account for the second largest product yield with 18.6 wt%, which can be broken down into 10.5 wt% ash and 8.1 wt% char. After pyrolysis, the solid products were separated from the quartz sand by sieving into fine, sand, and coarse fractions. This separation enables the sand fraction to be recycled for multiple use in pyrolysis experiments after thermal regeneration at 550 °C.

To gain more insight into the recycling possibilities of the coarse fraction, it was separated into a first coarse fraction with a particle diameter between 2 and 3.15 mm and a second coarse fraction with a particle diameter bigger than 3.15 mm. The latter consists of 81 wt% glass, magnetic metals, non-magnetic metals and wires which indicates potential for their material recovery after pyrolysis. This recovery of highly valuable metals creates additional economic value and ecological benefits. However, the separation and sorting of the coarse fraction must be automated and validated for technical feasibility on a larger scale, and a closed-loop implementation for the first coarse fraction needs to be identified.

The material recovery from the fine fraction seems unfeasible due to its inhomogeneous composition, measured using XRD. Calcite, rutile, and talc make up 83 wt% of the fine fraction and can be attributed to the mineral components of plastics, i.e., fillers. Quartz and K-feldspar in the fine fraction presumably originate from abrasion of the carrier material and thermal stress in the screw reactor. Alternatively, K-feldspar could also have been introduced as a filler.

The XRF results of the fine fraction reflect the phase composition. In particular, the values for calcium (calcite), magnesium (talc), titanium (rutile), and silicon (quartz) are representative of this. The metal components in the pyrolysis residues lead to high and significant levels of chromium, manganese, iron, copper, zinc, and some typical steel alloy elements such as tungsten and niobium. The low content of halite (NaCl) and the lack of evidence of inorganic bromine compounds by XRD prove that a considerable proportion of chlorine (4 wt%) and bromine (0.4 wt %), measured by elemental analysis, is bound to organic carbon compounds (char).

Moreover, the elemental analysis of the fine fraction also showed a carbon content of 21 wt%, which indicates that it needs to be incinerated for further use.

Landfilling as disposal of the material with a high filler and sand abrasion content is not permitted due to the increased char content of this fraction, which is determined in the European best available techniques requirements for a total organic content of smaller than 3 wt% [32]. Accordingly, energetic utilization of the remaining energy content appears advisable. After suitable post-processing, the resulting mineral incineration residues may be reused as filler or sorbents.

5.3. Gaseous products

Gaseous products account for 13 wt% of product yield. However, those gaseous products were diluted to 4.2 vol% by the high amount of nitrogen needed to ensure an inert atmosphere. Despite the large number of compounds in the gas phase, it was possible to quantify approximately 1.6 vol% of its compounds. Nevertheless, a significant share of the total gas composition is not identified. These gases might be non-detectable heteroatomic components such as HCl, HBr, NH_3, or aromatic and aliphatic structures that pass through the condensation path due to their partial pressure or as a slip flow.

Including the HSI analyses, the detected components in the pyrolysis process can be evaluated. Unsaturated hydrocarbons and CO_2 dominate the gas composition. About 42 wt% of the identified gases are comprised of CO_2, reflecting the presence of oxygen. The pyrolysis of PC is known for its selective generation of CO_2 [33]. This aligns well with the detected PC-based compounds in the feedstock using combined SWIR-MWIR HSI analysis. Another reason for CO_2 presence may be the minor amounts of PET (0.2 %) and biomass impurities, such as wood (0.2 wt%) [34].

Complementary alkanes and alkenes were identified in the gas. These products can originate from the pyrolysis of various types of plastic. Polyolefins such as PP, PE, PS, ABS, and the polyene intermediate from the first degradation stage of PVC pyrolyze into such hydrocarbons [24,35–37]. However, PS, ABS, and PVC primarily form aromatic structures during pyrolysis. This would support the hypothesis of unidentified components in the gas.

The C_2 to C_4 alkenes could be used as a raw material to synthesize new polymers [6]. However, this would require the separation of these compounds, which represents an economic challenge. If recovery of the gaseous compounds is economically feasible due to the integration into chemical network sites with gas purification units, it could also enable the energetic use of the residual CH_4 and the recovery of CO_2 in carbon capture and utilization applications or the utilization of the hydrocarbon-rich gas via catalytic upgrading for hydrogen production [38].

Another approach would be the energetic utilization of this gas, which has a lower heating value (LHV) of around 1829 kJ/kg_{gas}. With 13 wt% gas yield a feedstock-related gas LHV of 2909 ± 216 $kJ/kg_{feedstock}$ is determined. The minimal energy demand of the endothermic pyrolysis process can be estimated, according to Netsch et al. (2024) [20]. This energy demand ranges from 1575 to 2424 kJ/kg, strongly depending on the polymer. In the case of successful flush gas reduction, which is necessary for classifying the gas as flammable, as conducted by Honus et al. (2018) [39], a comparison of the LHV with the minimal energy demand shows the potential of recovering the energy input from the pyrolysis gas. The minimal energy demand does not include heat and conversion losses from the process. As a result, thermal recovery may be

suitable for partly covering the pyrolysis plant energy demand. A further significant advantage of energetic gas utilization is the conversion of potential pollutants in the gas phase [40].

5.4. Organic condensate

Various analytical methods were used to examine the condensate composition to define a potential application for the most important product fraction with its 64.2 wt% yield. For this purpose, gas chromatography, such as quantitative GC-FID analysis, qualitative 2D-GC–MS analysis, 1H NMR spectroscopy, and elemental analysis were performed.

Comparing the elemental content of feedstock and organic condensate enables the calculation of elemental recovery rates. This rate represents the amount of each element, referred to as the element's proportion in the feedstock.

About 70.0 ± 4.6 % of carbon and 62.7 ± 9.0 % of hydrogen from the feedstock was recovered in the organic condensate. About 44.0 ± 12.5 % of the feedstock's nitrogen was found in the organic condensate. The relatively high standard deviations can probably be attributed to the elemental analysis, as the value of 0.5 wt% nitrogen content in the organic condensate is close to the quantification limit of 0.1 wt%. Only 1.3 ± 0.3 % of chlorine and 5.6 ± 0.8 % of bromine from the feedstock were found in the organic condensate. This indicates that these halogens may selectively form gaseous or solid products. Other studies of the PVC and brominated flame retardant decomposition mechanisms highlight HCl and HBr formation during the first decomposition stage [27,29]. This effect explains the conversion of the low chlorine and bromine content in the organic condensate.

Using GC-FID, approx. 28 wt% of styrene could be found, which are typical decomposition products of PS [36]. Since styrene and BTEX (13 wt%) are important petrochemical compounds and make up more than a third of the organic condensate, the recovery of these components should be considered. Holtkamp et al. (2024) modeled a distillation of a pyrolysis condensate featuring a similar composition in two columns and 40 stages [41]. With an initial concentration of 30 wt% styrene, the product was enriched to 90 wt% styrene and 9.6 wt% o-xylene. Using life cycle assessment (LCA), they demonstrated that the styrene recovery route outperforms incineration with energy recovery regarding global warming potential. Therefore, the authors suggest the pyrolysis and styrene recovery route of PS-rich waste. Processes for obtaining other pure, valuable products from organic condensate using fractional distillation are described elsewhere [42].

^{1}H NMR analyses provide more insights into the 51 wt% of unquantified compounds from GC-FID analyses to understand how the condensate is composed. The analyses reveal that most components consist of aromatic structures; however, one-third of the protons can be assigned to aliphatic groups. Due to the integral measuring principle of ^{1}H NMR, it can be determined that more aliphatic hydrocarbons are present in the organic condensate than the 1 wt% determined by GC-FID. These aliphatic hydrocarbons can either be *iso*-alkanes and *iso*-alkenes in the range between C_5 and C_{21} or long-chain aliphatic hydrocarbons larger than C_{21}. However, when measuring the organic condensate with a variety of different compounds using 1H NMR, it must be taken into account that using allocations by chemical shift areas, as in this work, can lead to the overlap of different protons. Thus, an unambiguous classification of the functional groups cannot be guaranteed with absolute accuracy. This overlap of the chemical shift ranges can be observed in the styrene spectrum depicted in Fig. 11. The four characteristic peaks near a chemical shift of 6.3 ppm of the unsaturated group bound to the aromatic ring fall into the integration range of aromatics (6.3 to 8.7 ppm), although they should be classified as olefins. For pure compounds, the integration ranges can be adapted, but if a mixture of several compounds is measured, this reallocation of individual peaks cannot be carried out, which is why empirically determined ranges are utilized.

Using qualitative 2D-GC enables the resolution of the exact molecules, which confirm the primary components quantified via GC-FID. Moreover, higher aromatic compounds such as dimers (diphenyls) and trimers of styrene or phenyl naphthenes could be identified in the organic condensate. This reflects a typical pyrolysis spectrum of PS or styrene-based copolymers, such as ABS [36,37]. With 2,3-dimethyl-1-heptene, a PP-characteristic pyrolysis product emerges [35]. In addition, a very polar component, 4-phenyl-butyronitrile, is identified, which indicates ABS or other nitrile-containing co-polymers in relevant quantities in the feedstock. This result correlates well with the SWIR-MWIR HSI analysis and the GC-FID analyses. Due to the low PE content in the feedstock, only a low proportion of volatilized paraffins is expected, which is confirmed by the 2D-GC analysis [43]. Therefore, the pyrolysis spectrum determined in the 2D-GC shows excellent correlation with the polymer type composition of the feedstock detected via SWIR-MWIR HSI and results from the literature.

However, the high PMMA content detected in the feedstock was not reflected by 2D-GC analysis, as the characteristic main degradation product of PMMA, methyl methacrylate (MMA), was not found [44]. It is possible that MMA and short-chain ketones and aldehydes derived from PMMA co-elute with the solvent or other compounds like 4-phenyl-butyronitrile which would cause peak overlapping. The analysis of the organic condensate emphasizes the effectiveness of pyrolysis in converting mixed plastic polymers into valuable hydrocarbon products with different chemical characteristics. The NMR analysis reveals an aromatic and aliphatic character of the condensates, while gas chromatography can identify and quantify the well-known compounds from the pyrolysis of specific plastic types.

In terms of utilizing the organic condensate, distillation has been proposed to recover styrene. However, the distillation could be conducted in such a way that purified BTEX can also be obtained. The remaining byproduct could be upgraded in a petrochemical process, such as hydroprocessing or fluid catalytic cracking, into valuable petrochemicals or feedstock to synthesize plastics [45]. Alternatively, the distillation may be used to generate a hydrocarbon-rich fuel substitute. Such a fuel substitute may be introduced in steam cracking processes to produce light olefins and valuable aromatics. In all cases, the properties of the condensate or a fraction thereof must be verified to fulfill the specifications of the subsequent petrochemical processes. The focus should mainly remain on the proportion of heteroatoms, aromatics, and unsaturated paraffins.

6. Conclusions and outlook

This study evaluates the chemical recycling of a plastic-rich waste fraction from refrigerators as an example of a highly heterogeneous and contaminated WEEE feedstock. The recycling potential is estimated in terms of in-depth feedstock characterization and TGA. Pyrolysis in a screw reactor on pilot scale enables the generation of representative pyrolysis products. The yields of the gaseous, liquid, and solid products are derived with low deviation, allowing further calculations regarding LCA. All products are characterized in detail to examine potential utilization options concerning material recycling.

With a high yield of styrene accompanied by BTEX in the organic condensate, pyrolysis followed by distillation appears promising to recover purified aromatic base chemicals. The base chemical enriched product fractions might be suitable for use in the chemical industry after upgrading to substitute fossil resources. The gas fraction and the solid residues feature product compositions challenging for further applications. The gas is rich in C_2 to C_4 alkenes. Such products may suit virgin polymer synthesis when purified. Heteroatom-containing pollutants complicate the gas separation. Alternatively, thermal utilization of the pyrolysis gas can cover energy requirement of the pyrolysis process and eliminate pollutants. Inorganic materials and char are enriched in the fine fraction from the sieving of the solid residue. The reuse of mineral residue with high filler content is to be verified. The sand fraction can be

reused as carrier material after thermal regeneration. The coarse fraction offers metal recycling options since the metal content of the feedstock is enriched in this product fraction. The metals can be separated from the glass with relatively low effort and may contribute to a significant economic benefit. A detailed concept of filler recycling and pollutant treatment from the solid residue is pending and needs to be proven.

The analytical methodology introduced in this work highlights the most critical feedstock characteristics needed to conceptualize potential recycling options. In general, the pyrolysis of plastic waste opens numerous new recycling routes for heterogeneous polymer-rich material. The technical feasibility, the ecological benefit compared to established waste treatment pathways, and the economic applicability of the presented options need to be further investigated separately for different feedstocks, as other WEEE feedstocks may result in other product yields and compositions. Specifically, more research about the utilization of pyrolysis oil distillation cuts and their upgrading is necessary.

CRediT authorship contribution statement

Jonas Vogt: Writing – original draft, Methodology, Investigation, Data curation, Conceptualization. **Axel D. Renno:** Writing – original draft, Methodology, Investigation, Data curation, Conceptualization. **Margret Fuchs:** Writing – review & editing, Writing – original draft, Investigation, Formal analysis, Data curation. **Tim Kurtz:** Writing – review & editing, Writing – original draft, Data curation. **Niklas Netsch:** Writing – review & editing, Writing – original draft, Data curation. **Frank Richter:** Writing – review & editing, Investigation, Formal analysis. **Grazyna Straczewski:** Writing – review & editing, Formal analysis, Data curation. **Britta Bergfeldt:** Writing – review & editing, Formal analysis, Data curation. **Yuleika Carolina Madriz-Diaz:** Writing – original draft, Methodology, Investigation, Data curation, Conceptualization. **Andréa de Lima Ribeiro:** Writing – review & editing, Formal analysis, Data curation. **Doreen Ebert:** Writing – review & editing, Formal analysis, Data curation. **Salar Tavakkol:** Writing – review & editing, Writing – original draft, Conceptualization. **Simone Raatz:** Writing – review & editing, Supervision, Resources, Project administration, Conceptualization. **Dieter Stapf:** Writing – review & editing, Supervision, Resources, Project administration, Conceptualization.

Declaration of competing interest

The authors declare that they have no known competing financial interests or personal relationships that could have appeared to influence the work reported in this paper.

Acknowledgements

This work was supported by the German Helmholtz Association through project-oriented funding in the program “Materials and Technologies for the Energy Transition”.

Additionally, we would like to thank Abrar Kabir, Rocco Naumann, Antonia Schneider, Roland Würkert, and Michael Stoll for their preparation of the samples. Ulrike Fischer, Cynthia Sanchez-Garrido, Norman Kelly, Patrick Schieber, and Krassimir Garbev assisted us with the chemical characterization of individual samples. Intensive discussions with Bradley Guy, Robert Möckel, and Martin Rudolph about the possibilities and limitations of the preparation and characterization of pyrolysis char were of enormous importance for this work.

Appendix A. Supplementary data

Supplementary data to this article can be found online at https://doi.org/10.1016/j.fuel.2025.135776.

Data availability

Data will be made available on request.

References

[1] Geyer R, Jambeck JR, Law KL. Production, use, and fate of all plastics ever made. Sci Adv 2017;3:e1700782. https://doi.org/10.1126/sciadv.1700782.
[2] Calabrò PS. Greenhouse gases emission from municipal waste management: The role of separate collection. Waste Manag 2009;29:2178–87. https://doi.org/10.1016/j.wasman.2009.02.011.
[3] Huang S, Wang H, Ahmad W, Ahmad A, Ivanovich Vatin N, Mohamed AM, et al. Plastic Waste Management Strategies and Their Environmental Aspects: A Scientometric Analysis and Comprehensive Review. Int J Environ Res Public Health 2022;19:4556. https://doi.org/10.3390/ijerph19084556.
[4] Yang Y, Boom R, Irion B, van Heerden D-J, Kuiper P, de Wit H. Recycling of composite materials. Chem Eng Process 2012;51:53–68. https://doi.org/10.1016/j.cep.2011.09.007.
[5] Paz FAG, Heibeck M, Parvez AM, Torrubia J, van den Boogaart KG, Raatz S. Recovery of materials from refrigerator: a study focused on product distribution. Recyclability and LCA Evaluation Sustainability 2024;16:1082. https://doi.org/10.3390/su16031082.
[6] Ahmad Fauzi AA, Osman AF, Alrashdi AA, Mustafa Z, Abdul Halim KA. On the use of dolomite as a mineral filler and co-filler in the field of polymer composites: a review. Polymers 2022;14:2843. https://doi.org/10.3390/polym14142843.
[7] Xanthos M. Polymers and polymer composites. Functional fillers for plastics, John Wiley & Sons, Ltd; 2005, p. 1–16. doi: 10.1002/3527605096.ch1.
[8] Wiesinger H, Wang Z, Hellweg S. Deep dive into plastic monomers, additives, and processing aids. Environ Sci Technol 2021;55:9339–51. https://doi.org/10.1021/acs.est.1c00976.
[9] Pivnenko K, Granby K, Eriksson E, Astrup TF. Recycling of plastic waste: Screening for brominated flame retardants (BFRs). Waste Manag 2017;69:101–9. https://doi.org/10.1016/j.wasman.2017.08.038.
[10] Kusenberg M, Eschenbacher A, Djokic MR, Zayoud A, Ragaert K, Meester S, et al. Opportunities and challenges for the application of post-consumer plastic waste pyrolysis oils as steam cracker feedstocks: To decontaminate or not to decontaminate? Waste Manag 2022;138:83–115. https://doi.org/10.1016/j.wasman.2021.11.009.
[11] Wäger PA, Schluep M, Müller E, Gloor R. RoHS regulated Substances in Mixed Plastics from Waste Electrical and Electronic Equipment. Environ Sci Technol 2012;46:628–35. https://doi.org/10.1021/es202518n.
[12] Schade A, Melzer M, Zimmermann S, Schwarz T, Stoewe K, Kuhn H. Plastic Waste Recycling—A Chemical Recycling Perspective. ACS Sustainable Chem Eng 2024;12:12270–88. https://doi.org/10.1021/acssuschemeng.4c02551.
[13] Ragaert K, Delva L, Van Geem K. Mechanical and chemical recycling of solid plastic waste. Waste Manag 2017;69:24–58. https://doi.org/10.1016/j.wasman.2017.07.044.
[14] Anuar Sharuddin SD, Abnisa F, Wan Daud WMA, Aroua MK. A review on pyrolysis of plastic wastes. vol. 115. 2016. Doi: 10.1016/j.enconman.2016.02.037.
[15] Vollmer I, Jenks MJF, Roelands MCP, White RJ, van Harmelen T, de Wild P, et al. Beyond mechanical recycling: giving new life to plastic waste. Angew Chem Int Ed 2020;59:15402–23. https://doi.org/10.1002/anie.201915651.
[16] Hall WJ, Williams PT. Analysis of products from the pyrolysis of plastics recovered from the commercial scale recycling of waste electrical and electronic equipment. J Anal Appl Pyrol 2007;79:375–86. https://doi.org/10.1016/j.jaap.2006.10.006.
[17] Stallkamp C, Hennig M, Volk R, Stapf D, Schultmann F. Pyrolysis of mixed engineering plastics: Economic challenges for automotive plastic waste. Waste Manag 2024;176:105–16. https://doi.org/10.1016/j.wasman.2024.01.035.
[18] Alston SM, Arnold JC. Environmental Impact of Pyrolysis of Mixed WEEE Plastics Part 2: Life Cycle Assessment. Environ Sci Technol 2011;45:9386–92. https://doi.org/10.1021/es2016654.
[19] Wang R, Xu Z. Recycling of non-metallic fractions from waste electrical and electronic equipment (WEEE): A review. Waste Manag 2014;34:1455–69. https://doi.org/10.1016/j.wasman.2014.03.004.
[20] Netsch N, Zeller M, Richter F, Bergfeldt B, Tavakkol S, Stapf D. Energy demand for pyrolysis of mixed thermoplastics and waste plastics in chemical recycling: model prediction and pilot-scale validation. ACS Sustainable Resour Manage 2024;1:1485–92. https://doi.org/10.1021/acssusresmgt.4c00109.
[21] DIN 51732:2014-07, Prüfung fester Brennstoffe_- Bestimmung des Gesamtgehaltes an Kohlenstoff, Wasserstoff und Stickstoff_- Instrumentelle Methoden n.d. Doi: 10.31030/2151764.
[22] Skoog DA, Leary JJ. Instrumentelle Analytik: Grundlagen - Geräte - Anwendungen. Springer-Verlag; 2013.
[23] Hesse M, Meier H, Zeeh B. Spektroskopische Methoden in der organischen Chemie. Thieme; 2012.
[24] Ma S, Lu J, Gao J. Study of the low temperature pyrolysis of PVC. Energy Fuels 2002;16:338–42. https://doi.org/10.1021/ef0101053.
[25] Takeoka Y. Poly(vinyl chloride) (PVC). In: Kobayashi S, Müllen K, editors. Encyclopedia of Polymeric Nanomaterials, Berlin, Heidelberg: Springer; 2021, p. 1–3. Doi: 10.1007/978-3-642-36199-9_247-1.
[26] Marongiu A, Faravelli T, Bozzano G, Dente M, Ranzi E. Thermal degradation of poly(vinyl chloride). J Anal Appl Pyrol 2003;70:519–53. https://doi.org/10.1016/S0165-2370(03)00024-X.

[27] Yu J, Sun L, Ma C, Qiao Y, Yao H. Thermal degradation of PVC: A review. Waste Manag 2016;48:300–14. https://doi.org/10.1016/j.wasman.2015.11.041.
[28] Zhao Z, Liu H, Gao W, Tian Y, Fa Y, Li G, et al. Screening of brominated pyrolysis products of tetrabromobisphenol a by integrating controllable heating device with ambient mass spectrometry. J Anal Appl Pyrol 2020;150:104896. https://doi.org/10.1016/j.jaap.2020.104896.
[29] Larsen ER, Ecker EL. Thermal Stability of Fire Retardants: I, Hexabromocyclododecane (HBCD. J Fire Sci 1986;4:261–75. https://doi.org/10.1177/073490418600400403.
[30] Bhaskar T, Murai K, Matsui T, Brebu MA, Uddin MA, Muto A, et al. Studies on thermal degradation of acrylonitrile–butadiene–styrene copolymer (ABS-Br) containing brominated flame retardant. J Anal Appl Pyrol 2003;70:369–81. https://doi.org/10.1016/S0165-2370(02)00183-3.
[31] Okeke ES, Huang B, Mao G, Chen Y, Zhengjia Z, Qian X, et al. Review of the environmental occurrence, analytical techniques, degradation and toxicity of TBBPA and its derivatives. Environ Res 2022;206:112594. https://doi.org/10.1016/j.envres.2021.112594.
[32] European Commission. Joint Research Centre. Best Available Techniques (BAT) reference document for waste incineration: Industrial Emissions Directive 2010/75/EU (Integrated Pollution Prevention and Control). LU: Publications Office; 2019.
[33] Antonakou EV, Kalogiannis KG, Stefanidis SD, Karakoulia SA, Triantafyllidis KS, Lappas AA, et al. Catalytic and thermal pyrolysis of polycarbonate in a fixed-bed reactor: The effect of catalysts on products yields and composition. Polym Degrad Stab 2014;110:482–91. https://doi.org/10.1016/j.polymdegradstab.2014.10.007.
[34] Wang S, Wang K, Liu Q, Gu Y, Luo Z, Cen K, et al. Comparison of the pyrolysis behavior of lignins from different tree species. Biotechnol Adv 2009;27:562–7. https://doi.org/10.1016/j.biotechadv.2009.04.010.
[35] De Amorim MTSP, Comel C, Vermande P. Pyrolysis of polypropylene: I. Identification of compounds and degradation reactions. J Anal Appl Pyrol 1982;4:73–81. https://doi.org/10.1016/0165-2370(82)80028-4.
[36] Faravelli T, Pinciroli M, Pisano F, Bozzano G, Dente M, Ranzi E. Thermal degradation of polystyrene. J Anal Appl Pyrol 2001;60:103–21. https://doi.org/10.1016/S0165-2370(00)00159-5.
[37] Day M, Cooney JD, Touchette-Barrette C, Sheehan SE. Pyrolysis of mixed plastics used in the electronics industry. J Anal Appl Pyrol 1999;52:199–224. https://doi.org/10.1016/S0165-2370(99)00045-5.
[38] Huang J, Veksha A, Foo Jin Jun T, Lisak G. Upgrading waste plastic derived pyrolysis gas via chemical looping cracking–gasification using Ni–Fe–Al redox catalysts. Chem Eng J 2022;438:135580. https://doi.org/10.1016/j.cej.2022.135580.
[39] Honus S, Kumagai S, Fedorko G, Molnár V, Yoshioka T. Pyrolysis gases produced from individual and mixed PE, PP, PS, PVC, and PET—Part I: Production and physical properties. Fuel 2018;221:346–60. https://doi.org/10.1016/j.fuel.2018.02.074.
[40] Schwartz NR, Paulsen AD, Blaise MJ, Wagner AL, Yelvington PE. Analysis of emissions from combusting pyrolysis products. Fuel 2020;274:117863. https://doi.org/10.1016/j.fuel.2020.117863.
[41] Holtkamp M, Renner M, Matthiesen K, Wald M, Luinstra GA, Biessey P. Robust downstream technologies in polystyrene waste pyrolysis: Design and prospective life-cycle assessment of pyrolysis oil reintegration pathways. Resour Conserv Recycl 2024;205:107558. https://doi.org/10.1016/j.resconrec.2024.107558.
[42] Wiriyaumpaiwong S, Jamradloedluk J. Distillation of pyrolytic oil obtained from fast pyrolysis of plastic wastes. Energy Procedia 2017;138:111–5. https://doi.org/10.1016/j.egypro.2017.10.071.
[43] Faravelli T, Bozzano G, Colombo M, Ranzi E, Dente M. Kinetic modeling of the thermal degradation of polyethylene and polystyrene mixtures. J Anal Appl Pyrol 2003;70:761–77. https://doi.org/10.1016/S0165-2370(03)00058-5.
[44] Kaminsky W, Eger C. Pyrolysis of filled PMMA for monomer recovery. J Anal Appl Pyrol 2001;58–59:781–7. https://doi.org/10.1016/S0165-2370(00)00171-6.
[45] Neuner P, Graf D, Netsch N, Zeller M, Herrmann T-C, Stapf D, et al. Chemical conversion of Fischer–Tropsch waxes and plastic waste pyrolysis condensate to lubricating oil and potential steam cracker feedstocks. Reactions 2022;3:352–73. https://doi.org/10.3390/reactions3030026.